EPAR V2.0: AUTOMATED MONITORING AND VISUALIZATION OF POTENTIAL AREAS FOR BUILDING RETROFIT USING THERMAL CAMERAS AND COMPUTATIONAL FLUID DYNAMICS (CFD) MODELS

Youngjib Ham[1] and Mani Golparvar-Fard[2]

[1] Ph.D Student, Department of Civil and Environmental Engineering, University of Illinois at Urbana-Champaign, Newmark Civil Engineering Lab, MC-250, 205 N. Mathews Ave., Urbana, IL 61801; PH (540) 235-6532; FAX (217) 265-8039; email: yham4@illinois.edu

[2] Assistant Professor, Department of Civil and Environmental Engineering, University of Illinois at Urbana-Champaign, Newmark Civil Engineering Lab, MC-250, 205 N. Mathews Ave., Urbana, IL 61801; PH (217) 417-9552; FAX (217) 265-8039; email: mgolpar@illinois.edu

Correspond to yham4@illinois.edu

ABSTRACT: This paper introduces a new method for identification of building energy performance problems. The presented method is based on automated analysis and visualization of deviations between actual and expected energy performance of the building using EPAR (Energy Performance Augmented Reality) models. For generating EPAR models, during building inspections, energy auditors collect a large number of digital and thermal imagery using a consumer-level single thermal camera that has a built-in digital lens. Based on a pipeline of image-based 3D reconstruction algorithms built on GPU and multi-core CPU architecture, 3D geometrical and thermal point cloud models of the building under inspection are automatically generated and integrated. Then, the resulting actual 3D spatio-thermal model and the expected energy performance model simulated using computational fluid dynamics (CFD) analysis are superimposed within an augmented reality environment. Based on the resulting EPAR models which jointly visualize the actual and expected energy performance of the building under inspection, two new algorithms are introduced for quick and reliable identification of potential performance problems: 1) 3D thermal mesh modeling using *k-d* trees and nearest neighbor searching to automate calculation of temperature deviations; and 2) automated visualization of performance deviations using a metaphor based on traffic light colors. The proposed EPAR v2.0 modeling method is validated on several interior locations of a residential building and an instructional facility. Our empirical observations show that the automated energy performance analysis using EPAR models enables performance deviations to be rapidly and accurately identified. The visualization of performance deviations in 3D enables auditors to easily identify potential building performance problems. Rather than manually analyzing thermal imagery, auditors can focus on other important tasks such as evaluating possible remedial alternatives.

Keywords: Building diagnostics; Thermography; Computational Fluid Dynamics (CFD); 3D reconstruction

1. INTRODUCTION

Today, increasing the efficiency of new and existing buildings and reducing their associated energy loss is getting more attention in the construction industry. The U.S. Department of Energy has estimated that home owners and facility managers can save 5-30% on their energy bills by making upgrades to their facilities [1].

Currently, space conditioning (i.e., heating, cooling, ventilation, and air-conditioning) is the largest single end-user of energy in non-industrial facilities [2]. To make the best use of the HVAC system, several factors such as building occupant's behaviors and appliance's energy efficiency need to be considered. Among these, one major factor which needs immediate attentions is to improve the condition of the building materials. The load on an HVAC system can be directly influenced by the poor thermal behaviors of buildings (e.g., thermal defects and air leakages in building envelopes) and in turn can cause the total building energy consumptions to be increased by more than 10 percent [3]. Today, roughly half of the entire building stocks in the U.S. (i.e., about 150 billion square feet of the existing buildings) suffer from such faulty behaviors and require renovation over the next 30 years to meet the higher energy standards. [4]. Yet, the current building diagnostic practices do not easily and accurately identify building performance problems such as insulation voids caused by building degradation. This limitation is also highlighted by the National Institute of Standards and Technology (NIST) as one of the top challenges associated with the current practices of building diagnostics [5].

In the meantime, infrared thermography as a reality capture method for sensing surface temperature variations

is gaining popularity among energy auditors. Nevertheless, identifying potential performance problems using thermal cameras for building retrofit is still challenging due to the following reasons:

(1) Thermal images captured from consumer-level thermal cameras typically have low spatial resolutions (160×120 or 320×240 pixels). As a result, modeling the whole building energy performance requires large numbers of thermal images. Not only auditors need to collect a large number of unordered imagery, but also they do not typically geo-tag each image they capture. Thus, it is difficult at a later stage to figure out what area these images are representing. Understanding what building components are associated with the performance problems detected in thermal imagery is a challenge for rapid building diagnostics. Quick and easy identification of the location and characteristics of the defects can minimize time and efforts required for diagnosis, and in turn enable auditors to spend more time on the retrofit decision-making.

(2) Current thermographic inspections are typically qualitative. Such analyses mainly focus on visual detection of the abnormal thermal regions such as hot and cold spots. Consequently, the knowledge and experience of the auditors can have a direct impact on the quality of the inspections [6, 7]. Due to the absence of energy performance benchmarks for comparison with the actual measurements, the current practice may adversely affect the diagnosis of performance problems, making it subjective and error-prone.

To address these challenges, this paper presents a new automated approach for quick and reliable identification of potential performance problems through a systematic and non-intrusive comparison of measured and simulated energy performance of a building. The proposed method for automated analysis and intuitive visualization of performance deviations builds on the recently prototyped EPAR modeling method [8] and leverages two emerging sources of information: (1) unordered collection of digital and thermal images collected using a single hand-held thermal camera with a built-in digital lens: these images enable the *actual energy performance* of the building under inspection to be modeled in 3D; (2) computational fluid dynamics (CFD) models: these models provide spatial distributions of the dynamic thermal performances and enable the *expected energy performance* to be modeled in 3D. Aiming at automated analysis and visualization of potential energy performance problems, this paper introduces two new algorithms: (1) 3D thermal mesh modeling using *k-d* tree and nearest neighbor searching; and (2) automated visualization of performance deviations in the EPAR models using a metaphor based on traffic light colors. In the following sections, first the state of knowledge is briefly reviewed. Next, the objective, the underlying algorithms, and computational processes are presented in detail. Finally, experimental results, the potential benefits, and limitations of the proposed method are addressed.

2. BACKGROUND

2.1 3D Thermal Modeling of Buildings

There have been many recent attempts in the building diagnostics research community to overcome the challenges associated with the application of large numbers of unordered and non-geo-registered thermal imagery. For example, the picture-in-picture function which is available for newer thermal cameras enables to pair thermal and digital images captured from the same location. Nonetheless, exploring large numbers of these overlaid 2D images for the purpose of entire building diagnostic can be time-consuming. To address this limitation, several researchers have focused on 3D thermal modeling of the building environments. In the AEC community, Cho and Wang [9] presented 3D thermal modeling of building façades using a hybrid LIDAR system which consists of a laser scanner and a thermal camera. This method generates the 3D laser scanning point clouds for building envelops and assigns temperature values to each reconstructed point. The proposed method has been extensively tested for the façade of a residential building, and promising results were presented. Similarly, Lagüela et al [6] introduced a methodology for registering temperature data with the 3D building point clouds generated using a terrestrial laser scanner. Im et al. [10] proposed a visualization method for 3D thermal models of building envelops on web-based geospatial systems such as Google Earth. Despite the effectiveness for surveying and modeling large-scale building exteriors and high measurement accuracies, using thermography with laser scanning for small interior spaces can be challenging. Recently, Lagüela et al. [11] outlined these challenges and proposed an image-based method for 3D building thermal modeling that can be used for indoor environments. Nonetheless, the proposed method involved several semi-automatic image registration and mosaic steps. Considering the large numbers of unordered thermal imagery, there is still a need for minimizing the time and effort required for semi-automated registration processes.

2.2 Building Performance Comparison using CFD Models

By solving the governing partial differential equations for mass, momentum, and energy conservation, the CFD analysis can predict the spatial distributions of thermal performance within each building zone [12]. Recently, the CFD analysis has been successfully applied to several energy performance studies for various indoor building environments [13, 14]. These works concentrated on comparison of the simulated thermal performance with the measured data captured by using thermocouples. Yet, identification of energy problems by comparing the CFD results and actual measurements still has the following challenges: (1) the state-of-the-art researches mainly use a limited number of designated locations for comparison purposes. The points-based comparison using only a few points does not comprehensively identify the areas that contain potential defects in a given space; (2) manual identification of the 3D locations of thermocouples in the CFD model may be prone to user selection error. Repeating the comparison for a large number of points

manually can also be very time-consuming and labor-intensive. To identify potential energy problems from performance deviations in a given space, there is still a need for a method that can automatically and accurately compare the actual and simulated energy performance of the building for the entire collection of points.

3. OVERVIEW OF THE PROPOSED METHOD

Given an EPAR model, formed by using a collection of unordered yet paired digital and thermal imagery as well as a CFD model, our goal is to create and validate a new method that can automatically calculate energy performance deviations and visualize potential problems in the EPAR model. The data and process in the proposed EPAR v2.0 modeling method are shown in Figure 1. Our approach mainly consists of four steps: (1) Generating 3D building and thermal point cloud models using two image-based 3D reconstruction pipelines [8]; (2) Simulating the building energy performance using the CFD analysis, and forming an expected 3D spatio-thermal model; (3) Superimposing the resulting actual and expected energy performance models in a common 3D environment, and generating the EPAR models; and finally (4) Automatically calculating and visualizing the performance deviations using new algorithms for 3D thermal mesh modeling and color coding based on the metaphor of traffic light colors. The following sections describe each of these steps in detail.

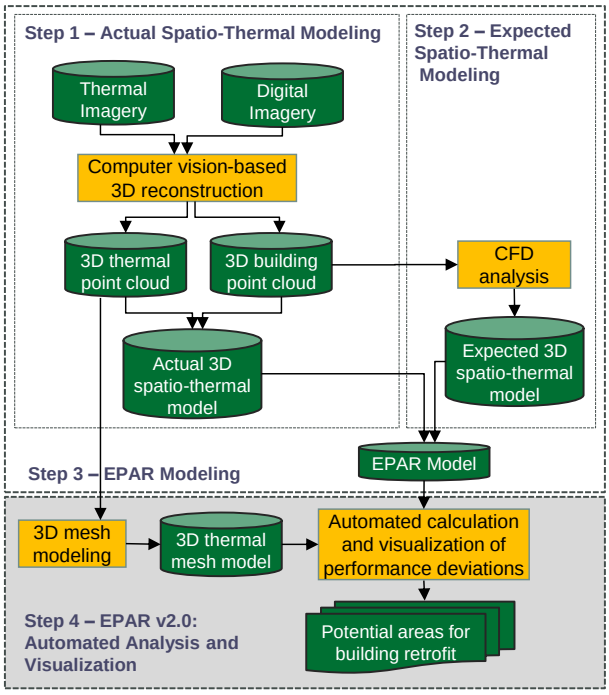

Figure 1. Overview of the proposed method

4. EPAR MODELING

4.1 Actual 3D Spatio-Thermal Modeling

We use a compute vision method known as Structure-from-Motion (SfM) to generate the 3D geometrical models of the buildings under inspection. The goal of the SfM process is to automatically estimate the extrinsic (e.g., locations and orientations) as well as the intrinsic camera parameters (e.g., focal length and radial distortion parameters). The SfM procedure involves the following four steps: (1) Detecting distinct feature points in each digital image: In this step, we use the graphic processing unit (GPU)-based implementation [15] of the scale-invariant feature transform (SIFT) algorithm [16] to reduce the computational cost. This method can rapidly find distinctive points invariant to possible changes in rotation, scale, and illumination for multiple images that are depicting the same object; (2) Matching the detected feature points across each image pairs. After capturing the intensity gradients of each feature point in form of a descriptor vector, feature descriptors in each image are matched using a nearest neighborhood matching algorithm. The Epipolar geometry between each image pair are then formed by estimating the Fundamental matrix (F) within random sample consensus (RANSAC) algorithm. Fitting F-matrix in the RANSAC loop helps eliminate false matches attributed to typically repeated visual features in building environments; (3) Initializing the 3D sparse reconstruction using an image pair which has the maximum matching features inliers after fitting F-matrix and the minimum matching features inliers after fitting a Homography matrix in the RANSAC loop. This constraint guarantees a high percentage of overlap and a wide baseline for the initial pair. Starting from the initial 3D reconstruction, the additional locations of the 3D points are incrementally calculated. The intrinsic and extrinsic parameters of the added cameras are also estimated using the Direct Linear Transformation (DLT) algorithm within the RANSAC loop [25]; (4) Once each camera is added, the camera parameters and the locations of the 3D points are finally optimized using bundle adjustment algorithm [17]. Here, we use the GPU-based sparse bundle adjustment library [18] to minimize the computational time. For more detailed process of the SfM algorithm, the readers are encouraged to look into [19, 20]. The outcomes of the GPU-based SfM algorithm are sparse 3D point clouds as well as the intrinsic and extrinsic digital camera parameters, which are fed into the dense 3D reconstruction step using Multi-View Stereo (MVS) algorithm [21]. For dense reconstruction, the features detected by Harris and Difference-of-Gaussians (DoG) operators are first matched across all images, returning sparse 2D patches which possibly contain several erroneous matches. Then, the expansion and filtering processes are iteratively executed to increase the density of the sparse 2D patches and eliminate false positives using the visibility constraints. The outcome of this step is a dense 3D point cloud model which represents the as-built conditions of the building under inspection.

The proposed method for 3D thermal modeling builds upon our recent research on reconstructing 3D building thermal models from unordered collections of thermal images [22]. Unlike digital images, infrared thermal images typically have low spatial resolutions. The lack of distinct features further challenges the application of the state-of-the-art feature detection techniques such as SIFT. As a result, there is a limitation to directly use the SfM algorithm for calculation of the camera parameters from

unordered thermal images. To overcome this, a new thermal camera calibration process is first formalized and implemented to estimate the intrinsic parameters of the thermal camera. To calibrate the camera, we use Bouguet's camera calibration toolbox [23] along with a calibration rig. The first step is to extract the grid corners of the calibration rig from the imagery. Because the thermal cameras are only capable of detecting infrared thermal variations emitted by the objects, the corners on the grid board cannot be clearly distinguished from the thermal imagery. To overcome this issue, we designed and put together a thermal calibration rig (550×700mm) with 42 small LED lights located on the grid intersections (δ=10cm). The LED lights emit enough heat to evidently distinguish themselves from the surrounding environment. For precise calibration, this increases the accuracy of extracting the grid corners from the thermal imagery (Figure 2). Before this step, the different temperature scales of each thermal image are normalized to a fixed range so that the each RGB color values in thermal imagery match an absolute temperature value.

Because we use a single thermal camera which has a built-in digital lens for data collection, we can estimate the extrinsic parameters of the thermal camera by calculating the relative pose of the thermal lens with respect to the digital counterpart. The Euclidean transformation between the thermal and digital lenses is calculated using Nistér's five point algorithm [24]. The location and orientation of each digital camera resulted from the GPU-based SfM algorithm is used as the baseline for calculation. First, the Essential Matrix is estimated by forming the Epipolar geometry between the digital and thermal lenses based on the selected five corresponding points. Then, the four candidates of the relative transformation metrics of the thermal lens with respect to the digital lens are recovered from the Singular Value Decomposition (SVD) of the Essential Matrix. The Cheirality constraint [25], as shown in the following, is used to determine the true configuration among the four candidates:

If $C_1 \equiv Q_3 Q_4 > 0$ and $C_2 \equiv (P_i Q)_3 Q_4 > 0$, then return P_i and Q

The selected corresponding points are triangulated using the DLT algorithm [25], resulting in reconstruction of the point Q in 3D. Here, Q_3 and Q_4 are the third and fourth components of the Homogenous coordinates of Q. Based on the extrinsic parameters of the digital camera ($[R_D|T_D]$) and the relative transformation metrics of thermal lens with respect to the digital counterpart $[R_{rel}|T_{rel}]$, the extrinsic parameters of thermal camera ($[R_T|T_T]$) are calculated through the following equation:

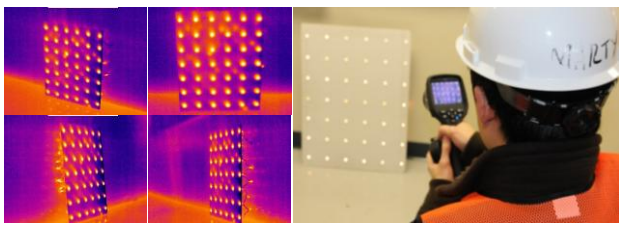

Figure 2. Thermal camera calibration

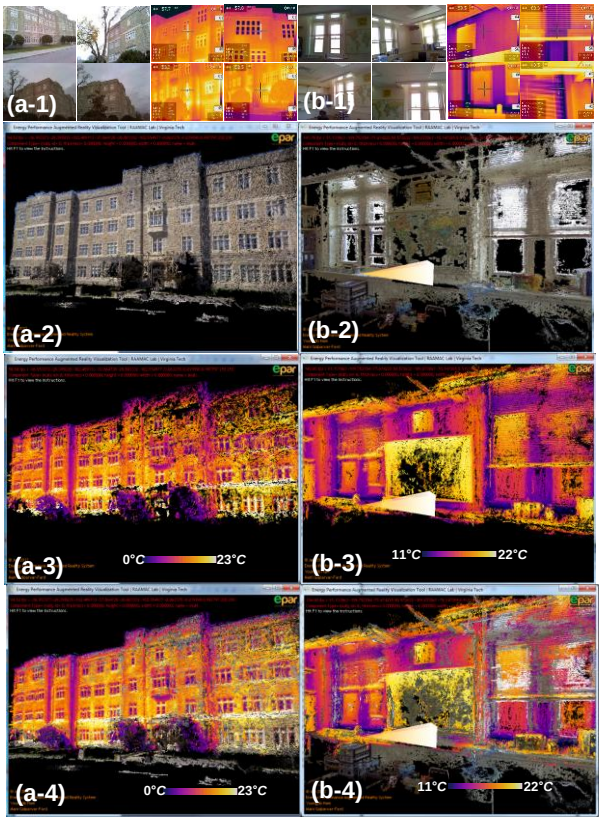

Figure 3. 3D spatio-thermal modeling

$$[R_T | T_T] = [R_D R_{rel} | R_D T_{rel} + T_D]$$

Once the thermal camera parameters are estimated, we use the same dense 3D reconstruction algorithm that was also used for 3D building geometrical modeling. The outcome of this step is a dense 3D thermal point cloud model of the building under inspection.

The final step for actual building energy performance modeling is to superimpose the generated 3D building and thermal point cloud models within a common 3D environment and form a 3D spatio-thermal model. Since the relative location and orientation of the thermal lens with respect to the digital counterpart were used as the extrinsic camera parameters for the 3D thermal modeling process, both of these models share the same coordinate system. Thus, the two models are automatically superimposed by carrying the both models into a single 3D virtual environment, generating the actual 3D spatio-thermal models. Figure 3 presents experimental results of the 3D spatio-thermal modeling on both indoor and outdoor built environments. In this figure, from top to bottom rows are: unordered digital and thermal imagery, the building point cloud models, the thermal point cloud models, and finally the integrated visualization of two models. The figure is best seen in color.

4.2 Expected 3D Spatio-Thermal Simulation

For geometrical modeling and the CFD analysis, we use Gambit 2.2.30 and Fluent 6.2.16 respectively. To create the 3D geometry, the boundary points (e.g., corners of windows) are manually extracted from the generated 3D dense building point clouds. Using the 3D coordinates

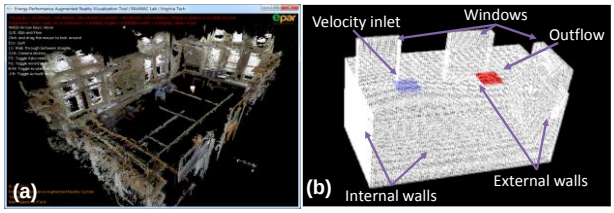

Figure 4. Meshing and specifying boundary condition

of each selected boundary point, the 3D wireframe model is created. The dimensions are calibrated based on the site coordinate system. The resulting calibrated 3D domain is divided into a series of small discrete mesh volumes (Figure 4). The interior surface temperatures resulted from EnergyPlus simulation, are fed into the CFD analysis as initial environmental boundary conditions. Exchanging the complementary data between EnergyPlus and CFD simulation can reduce the impact of the principal modeling assumptions employed in their separate applications, and thus can enable more accurate prediction of the building performance [26]. For the turbulence modeling, we use the renormalization group (RNG) $k-\varepsilon$ model [27]. The simulation specific parameters (e.g., the numeric convergence tolerances) are manually set by the users. Finally, by using Finite-volume method and energy conservation equations, the simulation is iterated for each 3D mesh element until the results are converged. After converging to a solution, the CFD analysis delivers the expected 3D spatio-thermal models which contain the simulated 3D thermal distribution.

4.3 Integrated Visualization of Actual and Expected Energy Performance

Overlaying the simulation results on the actual energy performance model can facilitate sensing and analyzing of the deviations between actual and expected energy performance of a building in 3D. For the integrated visualization, the display graphics of the CFD model is first converted to Virtual Reality Modeling Language (VRML) format, enabling export of 3D geometrical entities of the simulation results. Since image-based 3D reconstructed scenes are up-to-scale, we need to transform the actual 3D spatio-thermal models into the site coordinate system. To do that, we use the closed-form solution of absolute orientation using unit quaternions [28, 29]. In order to solve 7 DOF problem [3 for translation (T) + 3 for rotation (R) + 1 for uniform scale (s)], users need to select a minimum of three points from both the 3D spatio-thermal model and the real-world. Estimating the accurate registration is approximated with minimization of the sum of squared residual errors between the *n* corresponding pairs using the following equation.

$$\sum_{1}^{n}\left\|e^{i}\right\|^{2}=\sum_{1}^{n}\left\|r_{Site}^{i}-sR\left(r_{Model}^{i}\right)-T\right\|^{2}$$

The r_{Model}^{i} and r_{Site}^{i} denote the two sets of Cartesian points from the 3D spatio-thermal model and site coordinates respectively. Since the 3D geometry used for CFD analysis was also calibrated during the simulation process, both actual and expected performance models can be automatically superimposed within the same coordinate systems. The generated EPAR models along with the geo-tagged thermal and digital imagery jointly visualize the 3D actual and expected energy performance of the building under inspection.

5. AUTOMATED VISUALIZATION OF POTENTIAL PERFORMANCE PROBLEMS

5.1 3D Mesh Modeling of Actual Thermal Performance

In order to automatically identify deviations between the actual and expected energy performance of a building in a given space, we compare the measured and simulated indoor surface temperatures at the level of 3D points. To that end, we first define the following data sets:

- $(P_A^1, P_A^2, \ldots, P_A^m)$ denote a set of 3D actual thermal points based on the result of the image-based 3D reconstruction pipeline. $P_A^i =< X_A^i, RGB_A^i >$ encapsulates the 3D location (X_A^i) and the color (RGB_A^i) of each measured 3D thermal point, and *m* is the number of actual thermal points. Here, each RGB color value is corresponding to a fixed normalized temperature scale.
- $(P_S^1, P_S^2, \ldots, P_S^l)$ denote a set of 3D simulated thermal points resulted from the CFD analysis. $P_S^i =< X_S^i, RGB_S^i >$ encapsulates 3D location (X_S^i) and color (RGB_S^i) of each simulated 3D thermal point. *l* is the number of thermal points in the VRML-based CFD model. Each RGB color value is also corresponding to a fixed temperature scale.

Direct comparison of these two datasets is prone to error since it is nontrivial to find the closest pairs between the actual and simulated thermal points. The actual 3D thermal point cloud models typically include large numbers of points that do not belong to the building geometry itself. Thus, image-based 3D thermal point cloud models may not reveal the best representation of the actual thermal performance in a given space. To overcome this, we generate 3D mesh models of actual thermal performance using the VRML-based models as the geometrical baselines. Our approach for 3D mesh modeling of the actual thermal performance is to find the closest point P_A^i for each P_S^i and transfer the RGB color values of P_S^i to the corresponding P_A^i. To find the closest points for pairing, the brute-force method is to calculate the distance from the query point to every other point in the corresponding dataset, sort all the distances in an ascending order, and then choose the pair that yields the shortest distance. For the significant number of points in a cloud, this naïve method requires high computational time. To minimize computational time for finding the nearest neighbor, we map the points into a *k-d* tree structure. The *k-d* tree algorithm is an approach for space-partitioning data structure to organize points in a *k*-dimensional space [30]. The trees are used to store spatial data in a multi-dimensional space. The *k-d* trees recursively divide the set of points into subsets with half of the points of the parent node by using a plane through

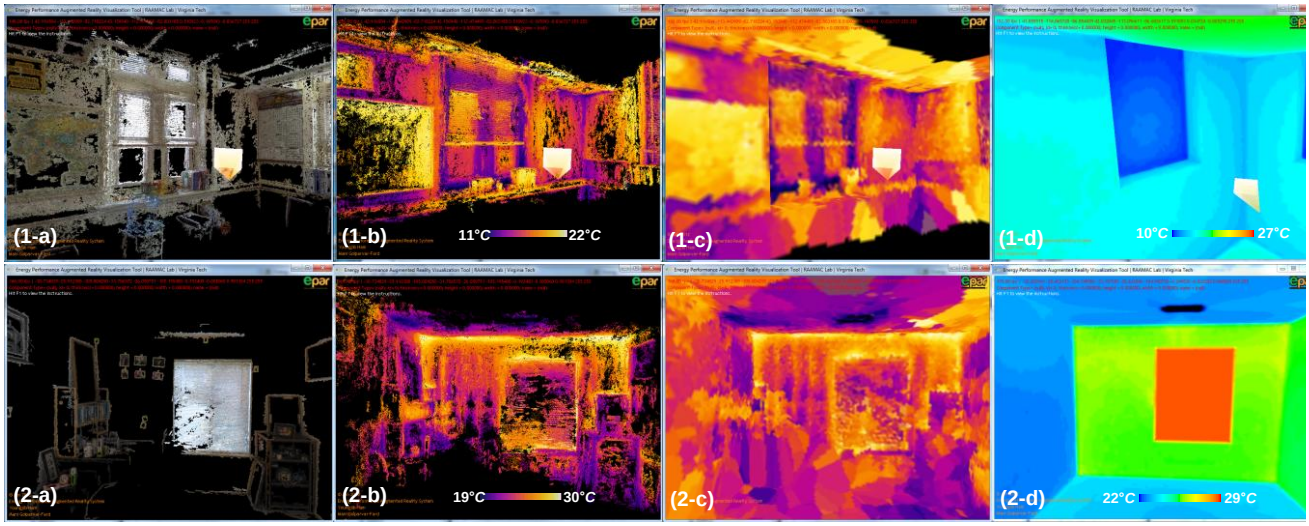

Figure 5. (a) and (b): 3D building and thermal point cloud models, (c): 3D thermal mesh models, (d): VRML-based simulated 3D spatio-thermal models (first row: Case #1, second row: Case #2). Figure is best seen in color.

one of the dimensions. The resulting point sets are again partitioned into equal halves using planes of a different dimension. Partitioning point sets stops after *log n* levels where *n* is the number of points in the set, and in turn each point locates its own leaf cell. Thus, the *k-d* trees hierarchically decompose overall space into a series of cells so that no cell contains too many points.

The nearest neighbor search with the *k-d* tree algorithm can be done efficiently by using these tree properties to eliminate a significant portion of the overall search space. To implement the nearest neighbor calculation, each tree is searched, and the nearest distance is approximately estimated at each stage. First, the root node is examined, and the sub-domain containing the target query point is searched. This process is recursively performed until the final minimum sub-domain containing the node is searched. Then, the algorithm looks into each parent node, and identifies other domain that may include a closer point. This process is repeated until all domains are either searched or discarded. Once the algorithm fails to find a possible closer point, the searching process is terminated and yields the nearest neighbor P_A^i. The RGB color value of the resulting nearest neighbor P_A^i is fed into the proposed mesh modeling algorithm.

5.2 Actual and Simulated Temperature Calculation and Comparison

Once actual and simulated 3D thermal mesh models are formed, the actual and simulated surface temperatures of a given space (T_A^i and T_S^i respectively) are calculated. First, the fixed temperature scales of both thermal imagery and CFD models (TS and CS respectively) are converted into a fixed range of the corresponding RGB color value (RGB_{TS} and RGB_{CS} respectively). As long as the color spectrum is kept the same, this is a one-time step and does not need to be repeated for different data collections. Next, given the RGB_A^i and RGB_S^i, we find the matching RGB color values in RGB_{TS} and RGB_{CS}. Finally, T_A^i and T_S^i are calculated using the following equations:

$$T_A^i = TS_{min} + (RGB_{TS}^i - 1) \times \frac{TS_{max} - TS_{min}}{Level_{TS} - 1}$$

$$T_S^i = CS_{min} + (RGB_{CS}^i - 1) \times \frac{CS_{max} - CS_{min}}{Level_{CS} - 1}$$

where TS_{max} and TS_{min} are the maximum and minimum values of thermal imagery temperature scale, and similarly CS_{max} and CS_{min} are the maximum and minimum values of CFD temperature scale. $Level_{TS}$ and $Level_{CS}$ indicate the range of each RGB chart converted from the temperature scales used for thermal imagery and CFD model respectively.

The final step of the process is to compute the deviations of two values and visualize them within the EPAR models using the metaphor based on traffic light colors. In the proposed method, the 3D actual and simulated thermal mesh models share the same coordinate system. This is because we used the geometry of VRML-based CFD models for 3D mesh modeling of the actual thermal performance. Thus, by simply computing the difference between T_A^i and T_S^i for each 3D point from the 3D mesh model, we can analyze the indoor surface thermal performance deviations.

6. EXPERIMENTAL RESULTS

6.1 Experimental Setup and Data Collection

In order to validate the proposed method, experiments were conducted on two indoor locations: an office room of an instructional facility during winter (Case #1) and a bedroom of a residential building during summer (Case #2). The digital and thermal images were captured using a FLIR E60 thermal camera which has a built-in digital lens. The technical specifications of the thermal camera and experimental setups for the CFD simulation are summarized in Table 1.

6.2 Results and Discussion

Figure 5a and b present 3D building geometrical and thermal point cloud models. Figure 5c and d show the 3D

Table 1. Camera technical data and initial boundary conditions for the CFD simulation

Items	Values
Digital image resolution	2048×1536 Pixels
Thermal image resolution	320×240 Pixels
Thermal sensitivity	0.05 *°C*
Thermal measurement accuracy	2°C or ±2% of reading
Turbulence model	RNG *k-ε* model
Temperature of Inlet Air (Case #1: Heating System)	32 *°C*
Temperature of Inlet Air (Case #2: Cooling System)	19 *°C*
Wood thermal conductivity	0.13 *W/m.K*
Concrete thermal conductivity	0.7 *W/m.K*
Glass thermal conductivity	0.96 *W/m.K*
Gypsum board thermal conductivity	0.17 *W/m.K*

mesh models of actual thermal performance and the VRML-based CFD models. As observed, even for the areas that are sparsely reconstructed, the 3D thermal mesh model provides detailed information on the actual thermal performance. Figure 6 show the example of a potential performance problem which is detected in the residential building (Case #2). Small deviations between actual measurements and simulation results are typically related to the inherent uncertainty in measurement and simulation, and thus can be expected. Considering the measurement accuracy of the FLIR E60 camera and typical accuracy of the CFD simulations for modeling indoor environments, the threshold for detection of potential performance problems was set to 2°C in these experiments. Based on the threshold, the areas with or without potential performance problems are color-coded with red and green colors respectively.

For example, figure 6a shows the area with potential performance problems (red area). These areas are originated from the deviations between the actual (6b) and expected (6c) thermal performance of the building. Thermal deviations that are above the defined threshold provide a feedback to the auditors on what areas require additional detailed performance analysis. In our case study, although the deviations between the measured and simulated temperatures for most areas were below the threshold, a few significant thermal deviations were observed. Considering the degradation level of the facility (built in the beginning of the 1980s), these discrepancies may be caused by construction defects or insulation voids. Thus, additional diagnostics are required to find the exact source of heat loss and their corresponding impact on the energy efficiency of the building. Once a registered camera is visited in the EPAR models, each camera frustum is automatically texture-mapped with the corresponding digital and thermal images. The user can easily change the viewpoint and select to view a full resolution images captured from a particular camera location. Figure 6d shows the geo-registered thermal image where the problems were observed. Through 2D thermographic inspection of the geo-registered thermal image in EPAR models, the detected potential performance problems can be qualitatively validated. Figure 6e shows the geo-registered digital image which is depicting the same areas. This represents the building semantics of the same areas captured in the thermal images. Overall, by (1) minimizing the time and efforts required to search for specific thermal images that contain performance problems; and (2) figuring out where the thermal images are captured from, the proposed method can assist with rapid building retrofit decision makings. Video demos are found at www.raamac.cee.vt.edu/epar.

7. CONCLUSIONS

Reliable and quick identification of energy performance problems is a critical step in improving the building energy efficiency. To support identification of potential performance problems in existing buildings, we presented a new approach for automated calculation and visualization of deviations between actual and expected energy performance of a building based on EPAR models. Within the resulting EPAR v2.0 environments, surface temperature deviations of buildings can be queried from the 3D thermal mesh models and visualized at the level of 3D points. The proposed method for automated

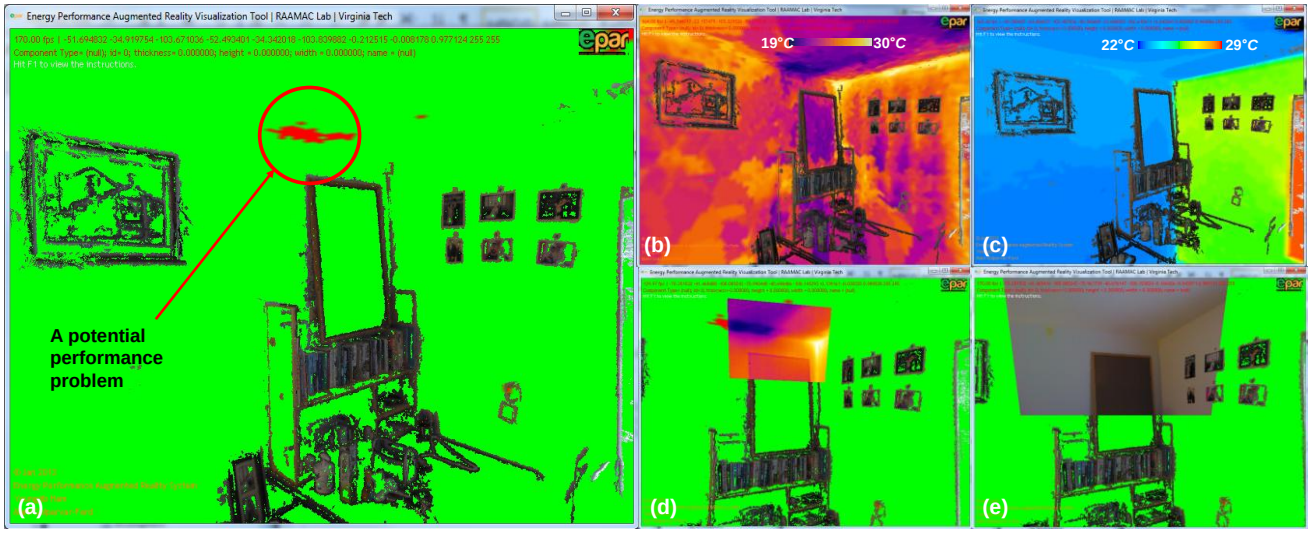

Figure 6. (a): visualization of a potential performance problem, (b) and (c): 3D thermal mesh model and VRML-based CFD model of the same area, (d) and (e): geo-registered thermal and digital imagery. Figure is best seen in color.

identification of potential performance problems can reduce the time and efforts required to analyze a large number of thermal imagery collected from the buildings under inspection. Moreover, this method enables building auditors to focus more on the other important tasks of assessing the observed problems and evaluating possible retrofit alternatives. Future works include converting the detected performance deviations into potential energy loss and the corresponding monetary savings. This can further motivate the building owners to renovate their facilities by helping them better understand the rate of the savings associated with the retrofit. There is also a need for identifying reliable thresholds for problem detection and eliminating false positives from the detected performance problems. The results of our ongoing research efforts will be presented in a near future.

REFERENCES

[1] U.S. DOE, "*Thermographic Inspections"*, < http:// www.doe.gov/energysaver/articles/thermographic-inspections>, *U.S. Dept of Energy*, 2012.

[2] U.S. DOE, "Energy Efficiency Trends in Residential and Commercial Buildings", *U.S. Dept of Energy*, 2008.

[3] Roth, K., Westphalen, D., Feng, M., Llana, P., Quartararo, L. "The Energy Impact of Commercial Building Controls and Performance Diagnostics: Market Characterization, Energy Impact of Building Faults and Energy Savings Potential", *TIAX LCC Technical Report* Cambridge, MA, 2005.

[4] Gould, K., Hosey, L. "Ecology & Design: Ecological Literacy in Architecture Education", *American Institute of Architects* (AIA), 2006.

[5] NIST, "Measurement Science Roadmap for Net-Zero Energy Buildings", *National Institute of Standards and Technology (NIST) Technical Note* 1660, 2010.

[6] Lagüela, S., Martínez, J., Armesto, J., Arias, P., "Energy efficiency studies through 3D laser scanning and thermographic technologies", *Energy and Buildings*, 43, pp. 1216-1221, 2011.

[7] Fokaides, P.A., Kalogirou, S.A. "Application of infrared thermography for the determination of the overall heat transfer coefficient (U-Value) in building envelopes", *Applied Energy*, 88, pp. 4358-4365, 2011.

[8] Ham, Y., Golparvar-Fard, M. "Identification of Potential Areas for Building Retrofit using Thermal and Digital Imagery, plus CFD Models", Proc., ASCE Int Workshop on Computing in Civil Eng, pp. 642-649, 2012.

[9] Cho, Y., Wang, C. "3D Thermal Modeling for Existing Buildings Using Hybrid LIDAR System", Proceedings of the 2011 ASCE International Workshop on Computing in Civil Eng, ASCE, Miami, Florida, pp. 68-68, 2011.

[10] Im, H.J., Gai, M., Wang, C., Cho, Y. "Hybrid Approach to Visualize Building Energy Information Model in Geospatial Application Programs", 2012 Construction Research Congress, pp. 1262-1270, 2012.

[11] Lagüela, S., Armesto, J., Arias, P., Herráez, J. "Automation of thermographic 3D modelling through image fusion and image matching techniques", *Automation in Construction*, 27, pp. 24-31, 2012.

[12] Zhai, Z., Chen, Q. "Solution characters of iterative coupling between energy simulation and CFD programs", *Energy and Buildings*, 35, pp. 493-505, 2003.

[13] Li, Q., Yoshino, H., Mochida, A., Lei, B., Meng, Q., Zhao, L., Lun, Y. "CFD study of the thermal environment in an air-conditioned train station building", *Building and Environment*, 44, pp. 1452-1465, 2009.

[14] Walker, C., Tan, G., Glicksman, L. "Reduced-scale building model and numerical investigations to buoyancy-driven natural ventilation", *Energy and Buildings*, 43, pp. 2404-2413, 2011.

[15] Wu, C. SiftGPU: A GPU implementation of Scale Invaraint Feature Transform (SIFT), 2007.

[16] Lowe, D. "Distinctive image features from scale-invariant keypoints", I*nternational Journal of Computer Vision*, 60, pp. 91-110, 2004.

[17] Triggs, B., McLauchlan, P., Hartley, R., Fitzgibbon, A. "Bundle adjustment- a modern synthesis", International Workshop on Vision Algorithms, Corfu, Greece, pp. 153-177, 1999.

[18] Wu, C., Agarwal, S., Curless, B., Seitz, S.M. "Multicore bundle adjustment", C*omputer Vision and Pattern Recognition*, pp. 3057-3064, 2011.

[19] Golparvar-Fard, M., Peña-Mora, F., Savarese, S. "Application of D^4AR- A 4-Dimensional augmented reality model for automating construction progress monitoring data collection, processing and communication", *ITcon*, 14, pp. 129-153, 2009.

[20] Snavely, N., Seitz, S., Szeliski, R. "Modeling the World from Internet Photo Collections", *International Journal of Computer Vision*, 80, pp. 189-210, 2008.

[21] Y. Furukawa, J. Ponce, Accurate, Dense, and Robust Multiview Stereopsis, *IEEE Transactions onPattern Analysis and Machine Intelligence*, 32, 1362-1376, 2008.

[22] Ham, Y., Golparvar-Fard, M. "Rapid 3D Energy Performance Modeling of Existing Buildings using Thermal and Digital Imagery", *Construction Research Congress*, West Lafayette, IN, pp. 991-1000, 2012.

[23] Bouguet, J.-Y. Camera Clibration Toolbox, 2010.

[24] Nister, D. "An efficient solution to the five-point relative pose problem, Pattern Analysis and Machine Intelligence", IEEE Transactions, 26, pp. 756-770, 2004.

[25] Hartley, R., Zisserman, A. *Multiple view geometry*, 2 ed., Cambridge University Press, 2004.

[26] Zhai, Z., Chen, Q., Haves, P., Klems, J.H. "On approaches to couple energy simulation and computational fluid dynamics programs", *Building and Environment*, 37, pp. 857-864, 2002.

[27] Yakhot, V., Orszag, S.A. "Renormalization group analysis of turbulence. I. Basic theory", *Journal of Scientific Computing*, 1, pp. 3-51, 1986.

[28] Horn, B., "Closed-form Solution of Absolute Orientation using Unit Quaternions", *Journal of the Optical Society*, 4, pp. 629-642, 1987.

[29] Golparvar-Fard, M., Pena-Mora, F., Savarese, S. "Integrated Sequential As-Built and As-Planned Representation with D^4AR Tools in Support of Decision-Making Tasks in the AEC/FM Industry", *J of Construction Eng and Mgnt*, 137, pp. 1099-1116, 2011.

[30] de Berg, M., Cheong, O., van Kreveld, M., Overmars, M. *Computational Geometry: Algorithms and Applications*, Springer, 2008.